73255

Aphanitic Impact Melt Breccia
St. 3, 394.1 g

INTRODUCTION

73255 is an aphanitic impact melt breccia that is unusual in being an oblate spheroid that has retained, to a large extent, the original shape and internal structures produced in the breccia-forming event. It is essentially an agglomeritic bomb with abundant clasts (Figs. 1-4). It consists of a clast-rich, non-vesicular, very fine-grained melt breccia core surrounded by a rind (up to 1 cm thick) of more vesicular, less clast-rich melt breccia that generally has a sharp contact with the interior (Figs. 3, 4). The core itself is an agglomeration of melt breccias. The chemical composition of the aphanitic melts is very similar to that of the common low-K Fra Mauro melt breccias that are generally assumed to be the Serenitatis impact melt, although it has lower TiO_2. The aphanitic melt crystallized at about 3.87 Ga, while older clasts such as pristine norites (one dated at 4.23 Ga), aluminous mare basalts, felsites, and feldspathic impactites are contained within it.

73255 was collected from the surface on the rim of a 10 m crater on the landslide at Station 3. Exposure appears to have occurred about 95 Ma ago, which is also the generally inferred age for the landslide itself. The sample is medium light gray (N5-N6), locally very light gray (N8), and is tough with a few penetrative fractures. It is 8 x 7.5 x 5 cm and surrounded. Its surface is rough and there are a few zap pits on most surfaces. Original surface is apparently present in some locations; in others the vesicular rind has been broken off. Macroscopically the sample appears to consist of about 85% matrix (less than about 100 microns), 10% lithic clasts, and 5% mineral clasts. A slab was sawn through the rock and most allocations were made from it. The sample was studied in detail in a consortium led by O. James.

PETROLOGY

The structure and petrology of 73255 have been studied in some detail. It consists of a core of non-vesicular aphanitic melt breccias (Fig. 5 a, b) enclosed in a rind of vesicular aphanitic melt breccia; all were created in a single impact

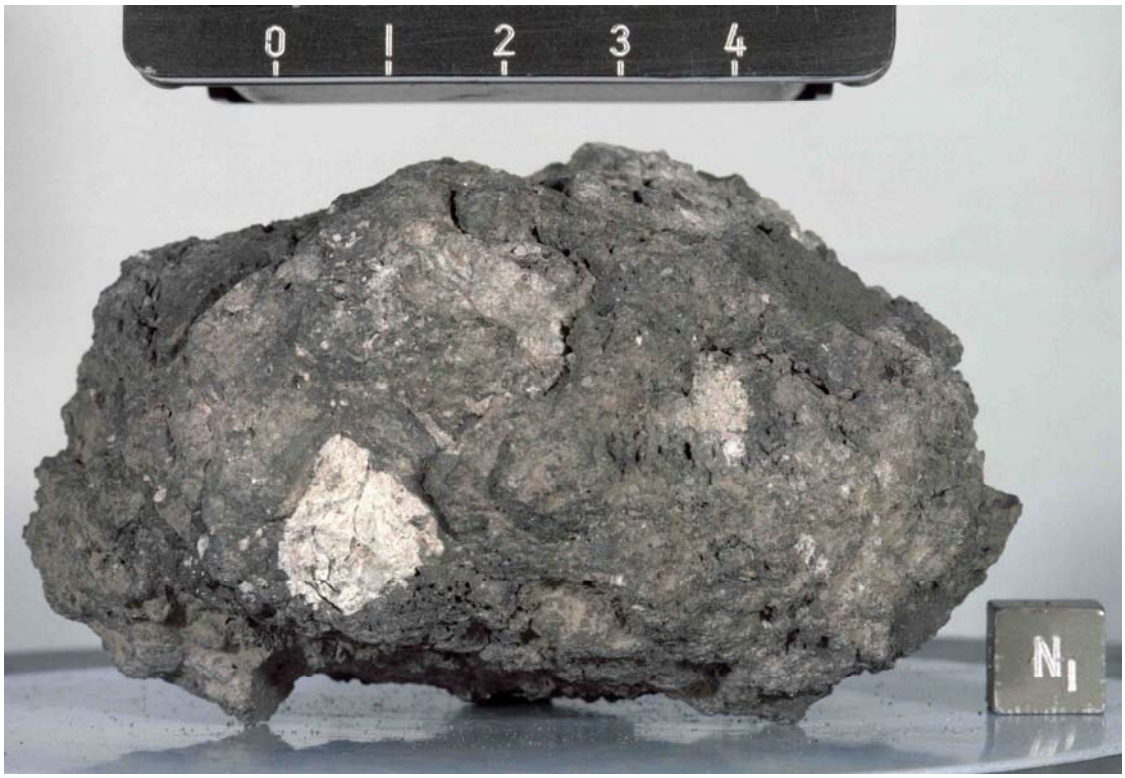

Figure 1: Pre-processing photograph of 73255, showing cindery appearance of vesicular rind and prominent lithic clasts. Cube is 1 centimeter. S-73-24202.

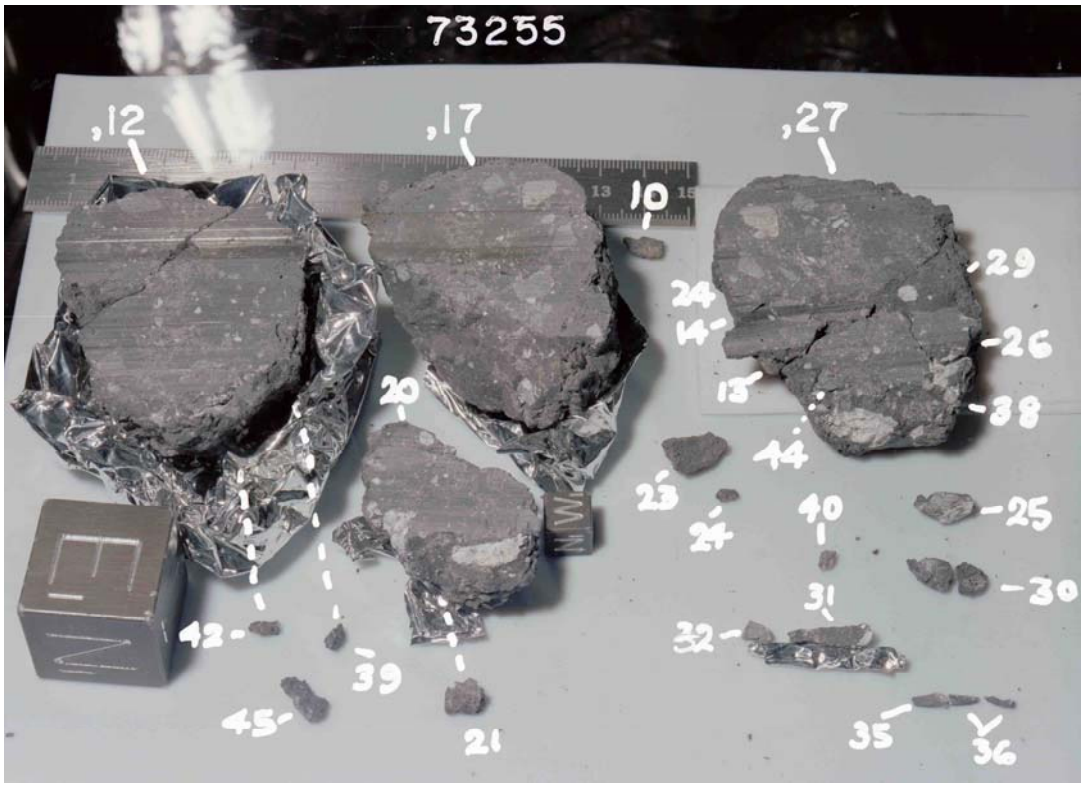

Figure 2: Photograph of 73255, post-slabbing, showing end pieces , 12 and,17 (and,20 which was part of the end piece), and the slab piece, 27 which has been subdivided Cube is 1 cm. S-74-22994.

Figure 3: Sawn surface of end piece, 17, showing large clasts and the distinct vesicular rind. Cube is 1 cm. S-76-25842.

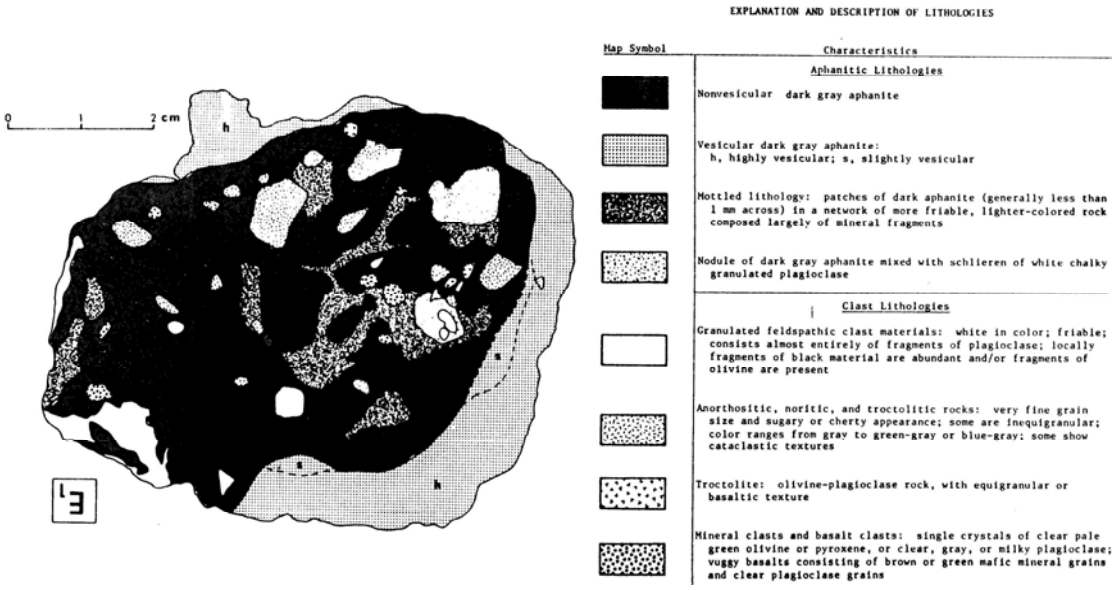

Figure 4: Lithologic map of one face of the slab cut through 73255, with key. From James et al. (1978).

event (James et al., 1978). All melt breccias contain mineral and lithic clasts, and the core aphanites include small cryptocrystalline globular masses. The cone contains abundant coherent lithic and mineral clasts, patches of friable white granulated plagioclase-rich rock, and mottled areas, as mapped by James et al. (1978) (Fig, 4). The clasts are from about 1 cm across down to the limits of resolution.

The general structure of 73255 and the petrology of the aphanitic melt breccias have been described and discussed by James et al. (1978), James and Marti (1977), James and Hedenquist (1978a), and Nord and James (1978 a, b), and were briefly discussed by Simonds et al. (1974) and Spudis and Ryder (1981), Two igneous norite clasts were described and discussed by James and McGee (1979a,b), and Nord and James (1979a,b). These two norites were described and used by James (1982) and James and Flohr (1982) as representatives of two main groups of pristine norites among lunar samples. Felsite clasts were described by James and McGee 09800 and Nord and James (1978a, b), and five mare basalt clasts were described by James and McGee (1980a, b). Brief descriptions of other clasts were given in James et al. (1978) and electron petrographic work on some anorthitic fragments was described in Nord and James (1978a, b).

James et al. (1978), James and Marti (1977), and James and Hedenquist (1978x) described the various lithologies, particularly the varied aphanitic melt breccias, and structure of 73255. They made a detailed study of four particular types of aphanitic melt breccia that dominate the rock: 1) non-vesicular core, 2) vesicular rind, 3) slightly vesicular material at the core-rind boundary, and 4) cryptocrystalline aphanitic melt that forms small particles within other aphanitic material in the core. The latter are most common in the mottled lithology of the core, in which the aphanites form irregular blebs and angular fragments. A summary of the characteristics of these four types is given in Table 1. The groundmasses are mainly subophitic to ophitic, and consist of plagioclase and pyroxenes, mainly 1-5 microns in dimension (Simonds et al., 1974, listed 1-10 microns for both phases, and suggested an "almost granular" texture). The grain size of the groundmass is finer than rock 73215, another aphanitic melt breccia collected nearby. Table 1 shows that the groundmass volume is varied from 59-85 volume % (virtually all melt-derived; clasts smaller than 5 microns have not been identified), and its abundance is roughly inversely correlated with grain size. The abundance of vesicles and their size are positively correlated. Defocused beam microprobe analyses show that the melt is close to the same composition in all melts (see CHEMISTRY section). There are virtually no post-consolidation shock features except some fractures, with no evidence of post-consolidation heating or shear.

The origin of the groundmasses as rapidly-cooled melts is shown in

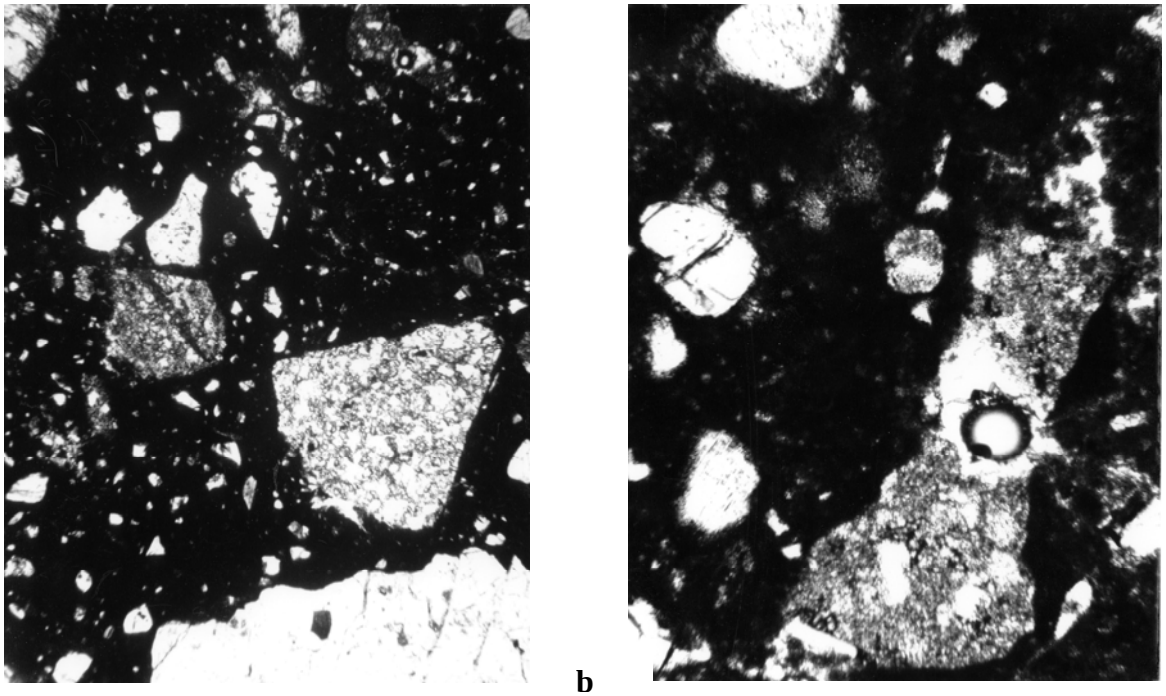

Figure 5: Photomicrographs of 73255,287, showing dense aphanitic groundmass and rounded to angular clasts Plane transmitted light. a) large plagioclase clast (bottom) and fine-grained feldspathic impactite (center left). Field of view about 2 mm wide. b) elongated fine-grained feldspathic impactite. Field of view about 500 microns wide.

electron petrographic (TEM) studies (Nord and James, 1978 a,b), in which the fine-grained subophitic/ophitic textures, with lath-shaped plagioclases, are clear. The plagioclases are a little more blocky in the more vesicular samples. Electron diffraction characteristics establish the pyroxene as pigeonite. These studies also found minor augite, but there was no orthopyroxene, olivine, or silica in the groundmass in the pieces investigated. Exsolution in the groundmass pyroxenes is of two types, as established in the TEM studies, and demonstrates rapid subsolidus cooling of the melt, and the absence of significant reheating after crystallization. Neither are there any shock-induced microstructures in the groundmass minerals, so there has been no significant post-consolidation shock event (>25kb).

Two norite clasts have been interpreted as being pristine igneous rocks. One, 27, 80 was 112 cm across, the other ,27,45, almost 1 cm in maximum dimension. Norite 27,80 is modally a pyroxene anorthosite with about 90% plagioclase and 10% orthopyroxene, but is probably an unrepresentative sample of a norite, whereas 27,45 has only about 50°% plagioclase. They are rather different in detail, and were used by James (1982) and James and Flohr (1982) as representatives of Mg-norites and Mg-gabbro norites respectively. Both cooled beneath the surface of the Moon, but in detail have different thermal and subsequent shock histories. They have been described in detail by James and McGee (1979a,b) and Nord and James (1979a,b) who provide petrographic (including TEM) descriptions and microprobe mineral analyses and have been subjected to other types of study (see CHEMISTRY and GEOCHRONOLOGY sections, below).

A thin section of pyroxene anorthosite 27, 80 consists of plagioclase (83%), orthopyroxene (15%), about 1% augite, 1% quartz + cristobalite, and less than 1% trace phases (James and McGee 1979a,b). The trace phases are K-feldspar, chromite, rutile, iron metal, apatite, whitlockite, baddelyite, armalcolite, troilite, ilmenite, and zirkelite. The texture is igneous, with equant plagioclase and pyroxene with sizes of 0.3 to 2 mm (most about 1 mm). The plagioclases have cores with inclusions (most almost certainly exsolved) and the orthopyroxenes have sparse, widely spaced thin augite exsolution lamellae and some exsolved oxides. The plagioclases are fairly homogeneous ($An_{93.1;}$ range $An_{91.1\text{-}95.3}$), as are the orthopyroxenes ($En_{72.9}Wo_{2.2}$) and clinopyroxenes (Fig. 5). The potash feldspars differ in composition from inclusions in plagioclase to interstitial phases (Fig. 7).The metal grains are extremely poor in Ni. The clast does have some well-developed shock-produced plastic deformation features, and the orthopyroxene has some patchy

Table 1: Characteristics of 73255 aphanites and 73215 aphanite. James et al. (1978).

	73255				73215[3]
	Cryptocrystalline	Nonvesicular	Slightly vesicular	Vesicular	Average of all types of matrix aphanite
Groundmass texture	Subophitic to devitrified-appearing; little intergranular porosity	Subophitic; locally variolitic or graphic; few percent intergranular porosity	Subophitic; locally variolitic or graphic; few per cent intergranular porosity	Subophitic with blocky pyroxene grains; locally variolitic or graphic; few percent intergranular porosity	Subophitic to intergranular; locally graphic or variolitic; intergranular porosity highly variable
Groundmass grain size	<1 μm	average ~2 μm (1–5 μm)	average ~2 μm (1–5 μm)	average 4–5 μm	average ~4–5 μm (<1–8 μm)
Vesicle content (vol.%)	~1–4[1]	~2[2]	~5[2]	21–34[2]	none
Vesicle size (mm)	average ~.01	average ~.01	average ~.02	average ~.04 range .01–1.0	—
Mode (vol.%, normalized to zero porosity)					
Groundmass	70–85[1]	72.3 (71.4–73.8)[2]	77.2[2]	66.4 (59.4–74.6)[2]	68.3 (65.7–71.1)
Plagioclase clasts >5 μm	not estimated	13.3 (7.9–18.0)[2]	10.3[2]	20.3 (11.6–25.4)[2]	22.5 (20.5–23.7)
Mafic-mineral clasts >5 μm	not estimated	7.4 (6.3–9.2)[2]	9.1[2]	9.6 (8.8–11.6)[2]	8.1 (5.1–10.9)
Lithic clasts >5 μm	not estimated	7.0 (1.4–13.6)[2]	2.8[2]	3.7 (2.7–6.3)[2]	1.1 (0–3.3)
Other clasts	not estimated	—	0.6[2]	—	—
Number of areas counted		(3)	(1)	(4)	(3)

[1]From visual estimates.
[2]From point counts on transparent overlays traced from reflected light photomicrographs of 0.6 × 1.4 mm areas.
[3]James (1976).

extinction. Fe-S rich glass veinlets have partly penetrated the clast during the 73255 breccia-forming event. Electron petrographic studies show heterogeneous microstructures in anorthites, the most striking of which are polygonal grains about 1 micron in diameter, other areas show recovery and defect-free patches. The potash feldspar inclusions have glass and some dislocations. The orthopyroxenes have 1000 angstrom-thick augite lamellae, and abundant stacking faults. The silica polymorphs show a wide range of shock features, including glass. The glasses in silica, anorthite, and K-feldspar indicate shock pressures of 250450 Kb; only the glasses in anorthite devitrified later. The only subsolidus, post-crystallization events, apart from shock, is the exsolution; the orthopyroxene exsolution suggests equilibration to 800 °C. The norite appears to have crystallized from an indigenous melt, slowly beneath the surface of the Moon. There are no recognizable xenocrysts and the

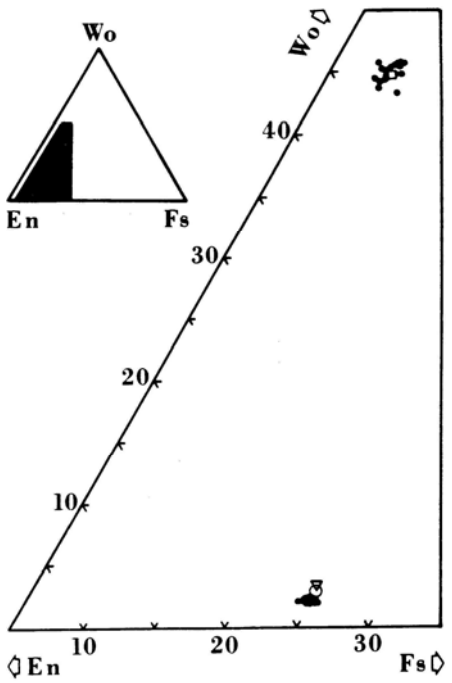

Figure 6: Compositions of pyroxenes in pyroxene anorthosite (norite) 27,80. See James and McGee (1979a) for details.

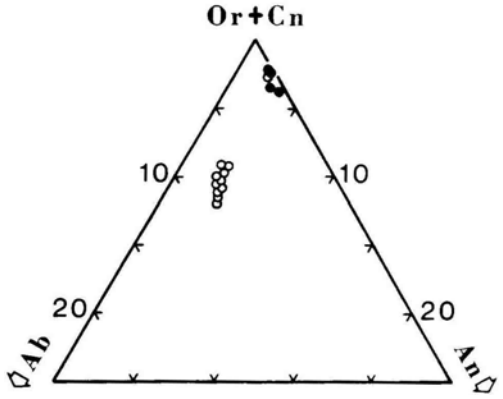

Figure 7: Compositions of potash feldspars in pyroxene anorthosite (norite) 27,80. Open circles are inclusions in plagioclase; filled are interstitial grains. James and McGee (1979x).

melt appears to have been rather evolved (to give an early plagioclase capable of exsolving K-spar and the many trace phases; see also CHEMISTRY). There may have been two generations of plagioclase growth.

Gabbronorite 27, 45 did not retain an igneous texture, although a few relict grain boundaries are preserved; instead it has a granulated texture, with a regular variation of intensity across the class Most grains are angular. Grains up to 1.8 mm and monomineralic areas suggest an original grain size of about 2 mm. James and McGee (1979a, b) gave a mode of 53% plagioclase, 40% orthopyroxene, 5% augite, 0.5% ilmenite, and 4.5% all other phases. The trace phases are apatite, whitlockite, chromite, troilite, iron-metal, stanfieldite (Ca-Mg-rich phosphate), armalcolite, and rutile. Single grains of K-feldspar and K-Si-rich glass were also found. The plagioclases do not contain inclusions, but the orthopyroxenes do contain inclusions as well as thin, widely spaced exsolution lamellae. The augites contain abundant exsolution lamellae of low-Ca pyroxene. Plagioclase compositions are fairly homogeneous ($An_{88.6}$, range $An_{86.7-90.5}$) and more sodic than in pyroxene anorthosite 27,80. The pyroxenes show significant correlation with texture, with exsolution lamellae differing from host grains of the same phase; individual grains are not zoned (Fig. 8). All of the iron metals, which seem to be part of injected veins, contain significant Ni (Fig. 9), unlike those in the pyroxene anorthosite 27, 80. Electron petrographic studies show that the bytownite is mainly defect free, with a low density of anti-phase domains. All pyroxenes contain exsolution, and orthopyroxenes have abundant stacking faults and Ca-enriched (GP) zones in varied density. The subsolidus effects indicate that the gabbronorite cooled at rates similar to the Bushveldt intrusion, down to 600 degrees C, and cooling to those temperatures in about 3000 years. This, with the compositional variation of pyroxenes, suggests cooling in the upper part of the lunar crust. The gabbronorite was shocked and granulated, with no significant production of thetomorphic glass, at about 50Kb, substantially lower than the shock pressures of 27, 80. This was accompanied by an Fe-S vapor. Only slight modification by post shock events occurred.

Two tiny felsite clasts were described with mineral analyses by James and McGee 0980c). One (27, 3) consists of a vermicular intergrowth of quartz and K-feldspar, with optically continuous quartz as ribs 15-45 microns thick. Shock has converted K-feldspar largely to glass, but original textures are preserved. The clast is cut by a veinlet of host aphanitic melt breccia, with reddish brown glass at the contact that is higher in SiO_2 and K_20 than host breccia. The plagioclase is rich in both K and Na ($An_{56.3}$ $Ab_{39.0}$ $Or_{4.7}$), and the K-feldspar is rich in Ba. Ca contents are higher in shock-vitrified K-spar than in non-vitrified K-feldspar. The other clast (253, 24) is more strongly shocked, although it originally had a similar texture of vermicular intergrowth of quartz and K-feldspar. The K-feldspar was converted completely to glass by shock and flowed. The contact with the surrounding breccia is marked by a band of devitrified glass. Neither clast displays textures unequivocally igneous or metamorphic in origin, but by comparison with a clast in 73215 is almost certainly igneous, The shock event(s) occurred prior to the incorporation of the felsites into the breccia, and melted and injected material into the clasts. At the time of incorporation into the breccia the clasts were hot or were heated at that time. Electron petrographic work on a separate (?) felsite was reported by Nord and James (1978a, b), although this felsite is similar to the others in having the same textures and shock glass in K-feldspar. The TEM studies confirm glass at the grain boundaries and within K-feldspar and a lack of glass in quartz. No microstructures indicative of deformation, or deformation followed by recovery, were observed in either the K-feldspar or the quartz. Pigeonite grains contain antiphase domain boundaries, abundant twins, and exsolved augite lamellae. Some glass at

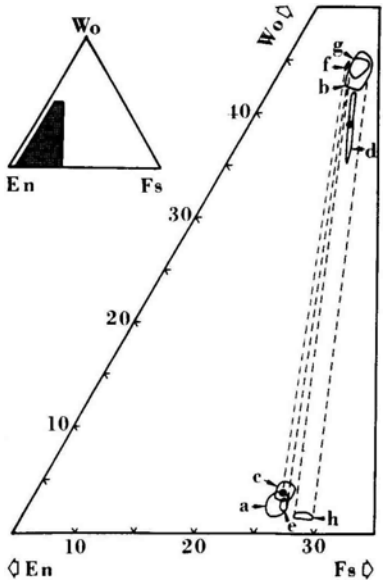

Figure 8: Compositions of pyroxenes in gabbronorite 27 ,45. For details see James and McGee (1979a).

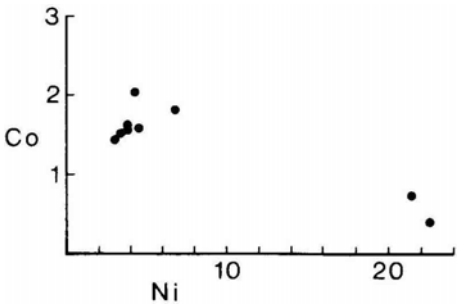

Figure 9: Ni-Co contents (wt%) of metal grains in gabbronorite 27,45. James and McGee (1979a).

grain boundaries was produced by beating within the breccia, not by direct shock heating, whereas K-feldspar glass shows characteristics indicative of both thermal and shock melting. Injection of veinlets and globules of mafic melt probably accompanied the shock event The evidence suggests that the clast was heated to more than 990 degrees C after incorporation into the breccia.

James and McGee (1980x, b) extracted five small mare basalt clasts from 73255, describing them and providing microprobe analyses. They are fractured and locally granulated; one is a collection of basalt fragments in a fine-grained matrix. The fragments are rounded and concentrated in the mottled lithology of the core. The basalts are generally subophitic but are all at least slightly different in grain size and texture; they probably form a sequence related by differentiation. The finest-grained fragment has some variolitic patches. Olivine and Cr-spinel crystallized first, followed by composite pyroxenes (pigeonite cores to ferroaugite rims) and plagioclase. Pyroxene and olivine analyses are shown in Fig. 10; these phases are iron-rich (e.g. olivine Fo <66) as they are in mare basalts. The plagioclases are calcic, averaging about An93. The basalts are high-alumina mare basalts, petrographically most similar to high-alumina mane basalt 14053. The granulation of the fragments appears to have taken place before the basalts had finished crystallizing; because the granulation appears to be a result of the shock event that produced the breccia, the basalts are inferred to be about 3.87 Ga old. The fragment consisting of basalts in a fine-grained matrix also has some patches of very fine-grained melt that is acuminous like the host aphanite.

Nord and James (1978a,b) reported electron petrographic studies of an undeformed anorthite (An_{97}; about 540 x 700 microns) and a shocked anorthite (An_{94}, 450 x 200 microns). anorthite showed no visible deformation in normal microscopy. The TEM studies showed a low dislocation density and unusually small type (c) antiphase domains; the former indicates no significant shock effects, the latter that the latest event was rapid cooling through 600 degrees C. The shocked anorthite had microscopically visible deformation lamellae and undulatory extinction. The TEM studies showed the presence of tiny crystallites, each with minute twin lamellae. The anorthite had been shocked into a glass and then devitrified, cooling rapidly, perhaps in two stages, to less than 840 ^{o}C.

The petrographic studies of the structure and lithologies of 73255 show that it crystallized from a mass of aphanitic melts of similar composition, including the vesicular rind, that contained numerous mineral and lithic clasts of varied shock history. All clasts were heated by the melt to above

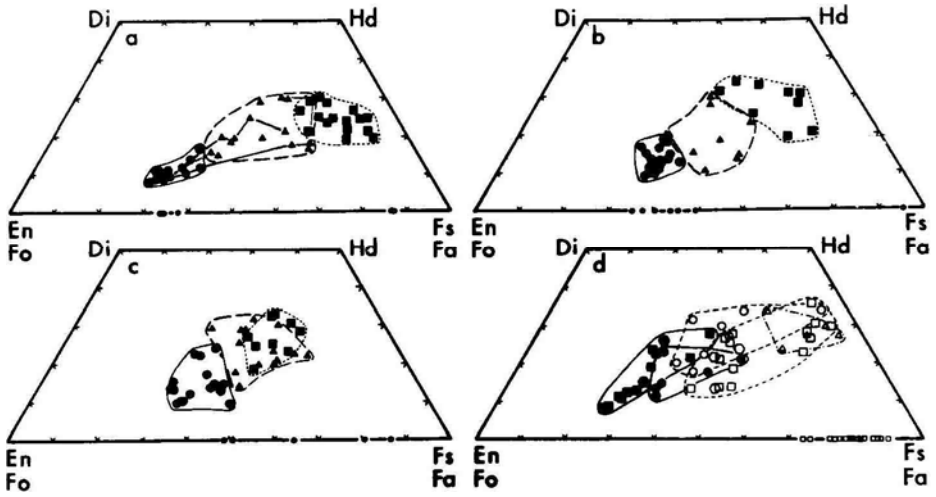

Figure 10: Compositions of pyroxenes and olivines in basalt clasts in 73255. Diagram d) contains data from 3 clasts: the others each are data from a single clast. James et al. (1980a).

900 degrees C and then cooled rapidly. Following crystallization, there were no significant shock effects.

CHEMISTRY

Major and trace element analyses of the bulk rock and aphanitic melt phases are compiled in Tables 2 and 3, with plots of the rare earths abundances in Fig. 11. A plot of rare earth abundances in comparative vesicular/non-vesicular aphanite pairs (James et al., 1978a) is given as Figure 12. Defocused beam microprobe analyses of the melt phase of the aphanitic melt phases are given in Table 4. Major and trace element analyses of separated clasts are given in Table 5, with a description of the clasts as analyzed by Blanchard and Budahn (1979x) given as Table 6. The rare earth element plots of Blanchard and Budahn (1979a) for different clast groups are presented as Fig. 13a-c. Mineral separates for pyroxene anorthosite (norite) 27,80, and not a bulk rock sample, were analyzed for trace elements by Blanchard and Budahn (1979a); the rare earth element plot for these separates and

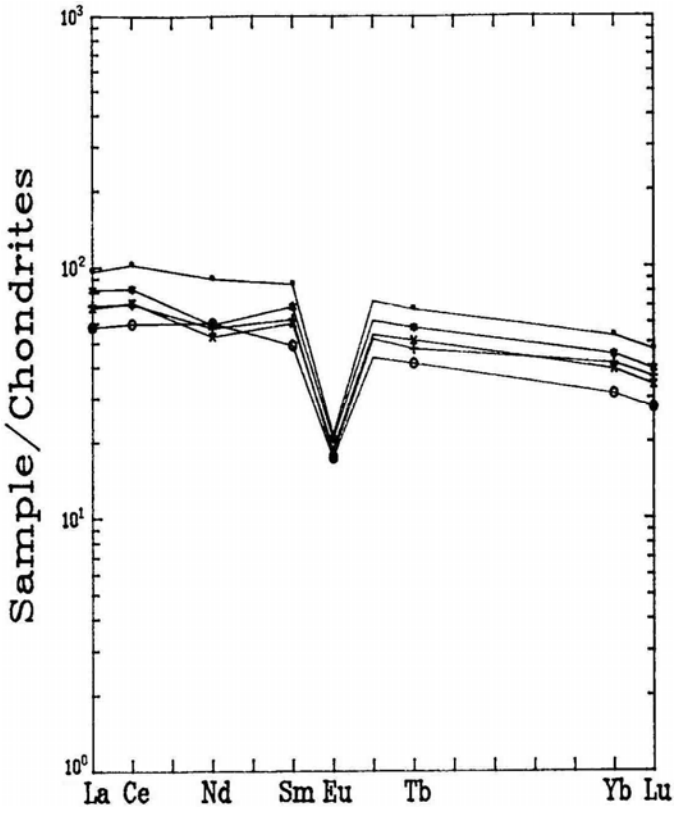

Figure 11: Rare earth elements in aphanites from 73255 (James et al., 1978).

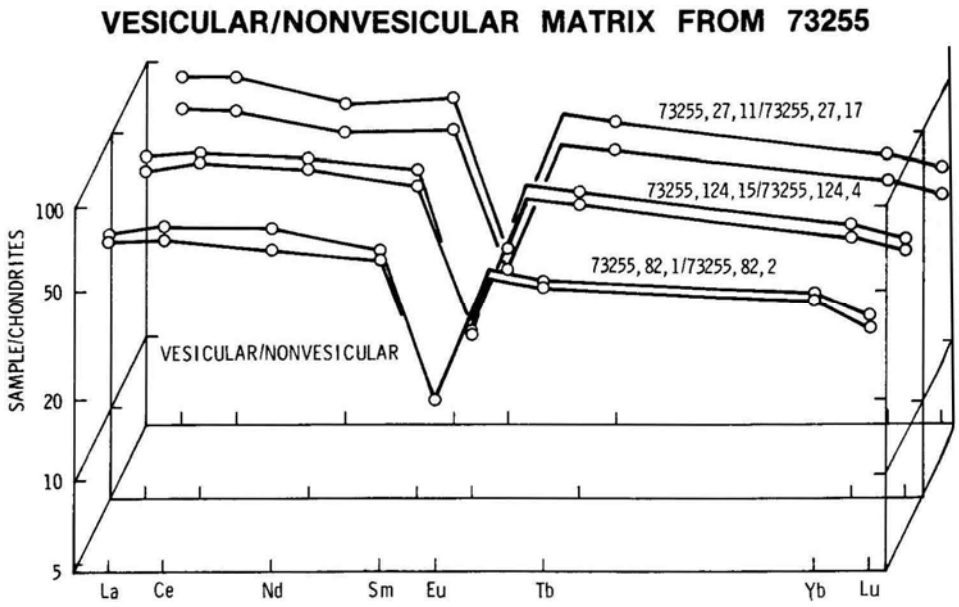

Figure 12: Comparison of rare earths in vesicular/non-vesicular aphanite pairs in 73255. (James et al. 1978).

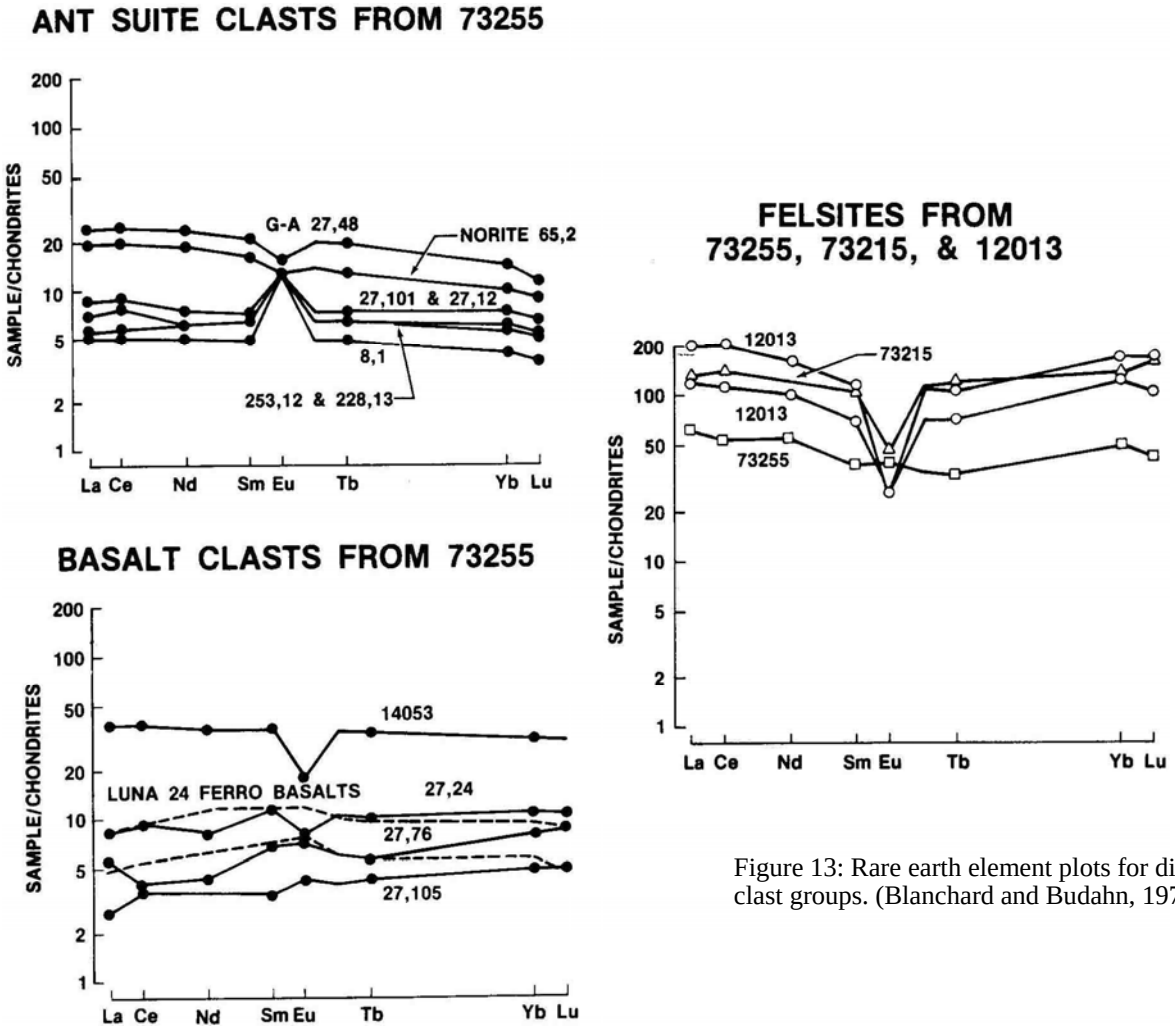

Figure 13: Rare earth element plots for different clast groups. (Blanchard and Budahn, 1979a).

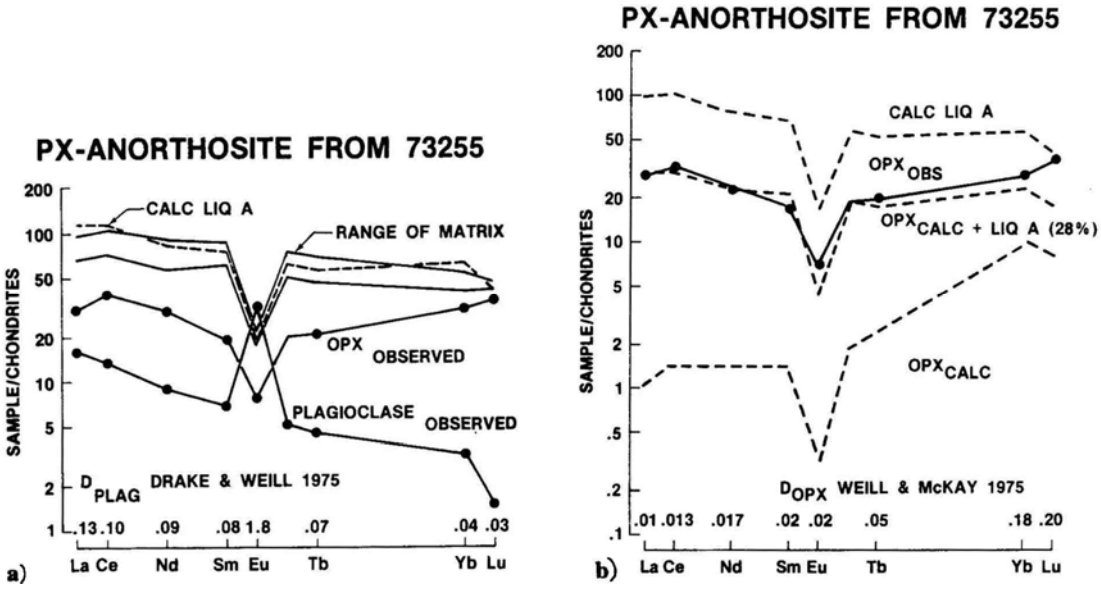

Figure 14: a) Rare earth element plots for mineral separates for pyroxene anorthosite (norite) 27, 80 and parent (LIQ A) calculated from plagioclase separate. b) Rare earth elements calculated for pure orthopyroxene and impure orthopyroxene separate for, 27, 80. (Blanchard and Budahn, 1979a).

calculated parent melts are given as Fig. 14a, b. The aphanitic melt breccia data show that the compositions cluster very tightly, more so than those in 73215, and are rather similar to other Apollo 17 fragment-laden melts, such as the Station 5 and 7 boulders. However, the 73255 aphanites do have lower TiO_2 (James et al., 1978, Blanchard et al., 1978). The 73255 aphanitic melts differ from others such as 73215 and the Boulder 1 Station 2 samples in being less feldspathic and having a lower dispersion of $A_{12}O_3$ and FeO among samples; however, most trace elements are virtually indistinguishable. The vesicular aphanites in 73255 appear to be slightly enriched in rare earth elements by about 10-30% compared with the non-vesicular aphanites (Table 3, Fig. 12). Other data suggests that the vesicular samples are enriched in some volatiles, such as Rb and Bi (Table 3). The aphanites are contaminated with meteoritic siderophiles and volatiles, corresponding with the Anders Group 2 assigned to Serenitatis rocks (Morgan and Petrie, 1979a, b).

Defocused beam microprobe analyses of the groundmass of the aphanites, avoiding clasts and thus corresponding with melt, indicate that the melt is fairly homogeneous and corresponds closely with bulk rock (Table 4). This indicates that the clast population has a bulk composition similar to that of the melt (James et al., 1978).

The gabbronorite clast 27,45 was analyzed as a tiny (10-12 mg) bulk samples (2 chips with different compositions) by Blanchard and Budahn (1979a, b) and for Sm and Nd by Carlson and Lugmair (1981). The coarse grain size makes these unrepresentative. The incompatible element contents are fairly low (Table 5, Fig. 13a) The norite has low enough Ni to be considered lacking in meteoritic contamination, although one of the subsamples has some black veins. The pyroxene anorthosite (norite) clast 27,80 was analyzed only for trace elements on mineral separates (Blanchard and Budahn, 1979a, b); the data indicates crystallization from an evolved parent with incompatible trace elements not unlike the host aphanite breccia; however, clearly the norite did not crystallize in place from such a parent.

The felsite sample analyzed was tiny (2.0 mg) and can hardly be representative. It is similar in major elements to the 73215 felsite and to 12013; it lacks the negative Eu anomaly of these others (Fig. 13b). Blanchard and Budahn (1978a, b) find their data indicative of an origin by liquid immiscibility.

The three basalt fragments analyzed (Blanchard and Budahn, 1978a, b) have major element compositions similar to high-alumina mare basalts, particularly Apollo 14 examples such as 14053, but the rare earth elements are more similar to very low-Ti mare basalts (Fig. 13c). The samples are generally similar but differ in detail; again, these are tiny analyzed pieces (less than 10 mg).

Table 2: Major and trace element chemistry of aphanite phases in 73255.

Split	,110 S	,148 N	,135,5 A	,253,13 B	,27,101 C	,122 V	,176 S	,245 N	,27,46 D	,0 E	Split
wt%											wt%
SiO_2	(47.5)	(47.9)	(47.0)	(48.6)	(46.8)						SiO_2
TiO_2	1.02	1.01	1.00	0.85	0.82						TiO_2
Al_2O_3	18.5	18.2	18.4	18.0	19.0						Al_2O_3
Cr_2O_3	0.31	0.36	0.34	0.34	0.32						Cr_2O_3
FeO	9.0	9.7	9.7	9.3	9.5						FeO
MnO	0.13	0.14	0.14	0.13	0.13						MnO
MgO	11.8	11.7	11.6	11.6	11.4						MgO
CaO	11.0	10.2	11.0	10.3	11.2						CaO
Na_2O	0.50	0.44	0.49	0.48	0.44						Na_2O
K_2O										0.191	K_2O
P_2O_5											P_2O_5
ppm											ppm
Sc	19.7	21.3	22.1	20.8	22.0						Sc
V	57	68	64	63	66						V
Co	28.2	33.7	30	33.1	29						Co
Ni	180	210	209	236	237				167		Ni
Rb											Rb
Rb (a)	9.93	5.31				9.85	5.54	5.28			Rb(a)
Sr	212	153	160	189	164						Sr
Sr (a)	126.1	122.8				128.6	125.4	118.1			Sr(a)
Y											Y
Zr											Zr
Nb											Nb
Hf	10.9	9.2	7.5	10.4	6.0						Hf
Ba	360	421	343	358	176						Ba
Th	5.6	4.0	3.9	4.6	2.9					3.47	Th
U									1.310	1.00	U
Cs											Cs
Ta	1.7	1.1	1.0	1.1	0.9						Ta
Pb											Pb
La	31.8	23.3	22.8	26.9	19.1						La
Ce	89.7	62.8	63.5	72.1	52.3						Ce
Pr											Pr
Nd	53.8	34.3	31.7	35.4	35.9						Nd
Sm	15.4	11.2	10.8	12.6	8.79						Sm
Eu	1.47	1.23	1.29	1.42	1.19						Eu
Gd											Gd
Tb	3.18	2.21	2.39	2.69	1.93						Tb
Dy											Dy
Ho											Ho
Er											Er
Tm											Tm
Yb	10.6	8.23	7.8	8.95	6.23						Yb
Lu	1.59	1.24	1.15	1.33	0.93						Lu
Li											Li
Be											Be
B											B
C											C
N											N
S											S
F											F
Cl											Cl
Br											Br
Cu											Cu
Zn									1.77		Zn
ppb											ppb
Au									3.0		Au
Ir									5.3		Ir
I											I
At											At
Ga											Ga
Ge									191		Ge
As											As
Se									87		Se
Mo											Mo
Te											Te
Ru											Ru
Rh											Rh
Pd									7.7		Pd
Ag									0.75		Ag
Cd									6.3		Cd
In									<2		In
Sn											Sn
Sb									2.0		Sb
Te											Te
W											W
Re									0.479		Re
Os									5.7		Os
Pt											Pt
Hg											Hg
Tl									1.99		Tl
Bi									<0.17		Bi
	(1)	(1)	(1)	(1)	(1)	(1)	(1)	(1)	(2)	(3)	

References and methods:
(1) James et a.l. (1978): INAA; (a) from ID/MS (a) also in Blanchard et al. (1978)
(2) Morgan and Petric (1979a,b); RNAA
(3) Eldridge et al. (1974a,b); Gamma ray spectroscopy.

Notes:
V = vesicular
N = non-vesicular
S = slightly vesicular, from core-rind contact
A = large globule in mottled lithology
B = coating on clast of granulated anorthosite
C = black fraction of black and white nodule
D = coating on granulated norite clast
E = bulk rock

Table 3: Major and trace element chemistry of comparative core-rind vesicular/non-vesicular aphanite melt phases in 73255. (James et al., 1978).

Split	,82,1 V	,82,2 N	,124,15 V	,124,4 N	,27,11 V	,27,17 N	,130 V	,124 N	Split
wt%									wt%
SiO_2	(48.4)	(48.0)	(47.0)	(45.6)	(48.1)	(47.1)			SiO_2
TiO_2	0.87	0.92	0.96	1.06	0.94	1.02			TiO_2
Al_2O_3	17.3	18.4	17.1	17.9	18.5	18.3			Al_2O_3
Cr_2O_3	0.35	0.33	0.40	0.35	0.33	0.35			Cr_2O_3
FeO	9.4	8.9	9.7	10.1	9.1	9.5			FeO
MnO	0.14	0.12	0.15	0.15	0.13	0.13			MnO
MgO	12.6	11.2	13.5	12.9	11.3	11.3			MgO
CaO	10.2	11.2	10.4	11.2	10.8	11.6			CaO
Na_2O	0.49	0.48	0.48	0.49	0.51	0.47			Na_2O
K_2O	0.25	0.34	0.27		0.27	0.14			K_2O
P_2O_5									P_2O_5
ppm									ppm
Sc	20.5	19.8	20.9	23.0	20.3	22.3			Sc
V	68	63	76	67	71	79			V
Co	27	26	27.4	28.2	25.2	29.2			Co
Ni	167	175	148	206	160	208	188	149	Ni
Rb									Rb
Rb(a)			(b)5.47	5.56					Rb(a)
Sr	131	145	140	150	140	160			Sr
Sr(a)			(b)126.0	127.3					Sr(a)
Y									Y
Zr									Zr
Nb									Nb
Hf	8.8	8.5	8.2	9.0	9.4	8.7			Hf
Ba	333	307	350	280	430	308			Ba
Th	4.3	4.1	4.3	4.3	4.8	3.6			Th
U							1.420	1.180	U
Cs									Cs
Ta	1.3	1.1	1.0	1.0	1.2	1.0			Ta
Pb									Pb
La	27.2	25.1	28.0	24.6	28.7	22.5			La
Ce	76.2	68.4	76.9	70.6	77.3	58.6			Ce
Pr									Pr
Nd	50.7	43.0	50	45	41.7	33			Nd
Sm	12.8	11.7	13.5	11.9	13.4	10.3			Sm
Eu	1.36	1.33	1.27	1.32	1.43	1.21			Eu
Gd									Gd
Tb	2.54	2.45	2.94	2.64	2.85	2.24			Tb
Dy									Dy
Ho									Ho
Er									Er
Tm									Tm
Yb	9.57	8.46	9.37	8.40	9.14	7.27			Yb
Lu	1.35	1.22	1.38	1.26	1.38	1.11			Lu
Li									Li
Be									Be
B									B
C									C
N									N
S									S
F									F
Cl									Cl
Br									Br
Cu									Cu
Zn							2.2	2.4	Zn
ppb									ppb
Au							3.2	2.4	Au
Ir							5.4	4.4	Ir
I									I
At									At
Ga									Ga
Ge							240	166	Ge
As									As
Se							91	81	Se
Mo									Mo
Te									Te
Ru									Ru
Rh									Rh
Pd							7.8	6.0	Pd
Ag							0.66	0.55	Ag
Cd							4.6	5.1	Cd
In							<3	<2	In
Sn									Sn
Sb							1.25	1.13	Sb
Te									Te
W									W
Re							0.482	0.383	Re
Os							5.6	5.2	Os
Pt									Pt
Hg									Hg
Tl							1.68	1.46	Tl
Bi							0.63	0.29	Bi
	(1)	(1)	(1)	(1)	(1)	(1)	(2)	(2)	

References and methods:
(1) James et al. (1978); INAA (SiO_2 by difference); (a) ID/MS (a) also in Blanchard et al. (1978)
(2) Morgan and Petrie (1979a,b); RNAA

Notes:
V = vesicular
N = non-vesicular
(b) analysis on slightly vesicular, core-rind contact

Table 4: Defocused beam microprobe analyses of clast-free groundmass areas of 73255. (James et al. (1478).

	73255[1]												
Section number	314(78)					9009(124)			280(171)			315 (158)	316 (265)
Analysis number	1	2	3	4	5	6	7	8	9	10	11	12	13
Type	C	NV	SV	V	BFC	SV	V	V(VAR)	NV(F)	NV(M)	NV(C)	C	NV
SiO_2	47.6	48.3	48.3	48.5	48.7	48.3	47.4	48.0	48.4	48.3	48.5	48.8	48.0
TiO_2	0.87	1.01	1.07	0.96	0.83	1.21	1.50	1.46	0.99	1.02	1.05	0.98	1.07
Al_2O_3	17.4	17.6	17.1	17.6	17.4	17.7	17.6	18.0	18.4	17.9	18.1	18.0	17.5
FeO	9.03	8.84	9.37	9.37	9.40	10.2	11.8	10.3	9.10	9.54	9.64	9.08	9.34
MnO	0.12	0.12	0.12	0.17	0.12	0.14	0.16	0.13	0.12	0.14	0.13	0.11	0.16
MgO	11.8	11.5	11.4	11.2	12.2	10.8	9.12	9.58	11.4	11.2	11.2	11.4	11.5
CaO	11.2	11.4	11.4	11.2	10.5	11.5	12.0	11.9	11.4	11.3	11.4	11.0	11.4
Na_2O	0.54	0.54	0.57	0.59	0.89	0.55	0.59	0.58	0.43	0.48	0.48	0.50	0.49
K_2O	0.30	0.38	0.40	0.47	0.57	0.36	0.37	0.38	0.27	0.26	0.29	0.33	0.32
Cr_2O_3	0.27	0.26	0.27	0.27	0.29	0.29	0.27	0.23	0.25	0.31	0.29	0.28	0.26
P_2O_5	0.20	0.21	0.23	0.22	0.17	0.16	0.16	0.22	0.21	0.21	0.25	0.22	0.19
Total	99.33	100.16	100.23	100.55	101.07	101.21	100.97	100.78	100.97	100.66	101.33	100.70	100.23
Number of spots analysed	15	11	15	8	4	10	10	10	11	10	12	7	3

	73255[1]										73215[2]		
Section number	286(265)			219(120)			Average C	Average NV	Average SV	Average V	Average black aphanitic matrix	Average gray aphanitic matrix	Average Schlieren-rich gray aphanitic matrix
Analysis number	14	15	16	17	18	19	(1 + 12	(2 + 9 − 11	(3 + 16	(4 +			
Type	C	NV	SV	SV	V	V(C)	+ 14)	+ 13 + 15)	+ 17)	18)			
SiO_2	47.6	47.7	48.1	48.7	48.5	48.7	48.0	48.2	48.4	48.5	47.6	46.7	48.1
TiO_2	0.99	1.05	0.98	1.09	1.08	1.08	0.91	1.03	1.06	1.03	1.00	1.09	1.04
Al_2O_3	18.3	17.5	17.5	18.3	17.4	18.7	17.6	17.8	17.6	17.5	19.0	19.0	18.0
FeO	9.49	9.71	9.27	9.37	9.52	8.61	9.08	9.41	9.35	9.45	8.26	8.27	8.73
MnO	0.13	0.13	0.11	0.13	0.14	0.17	0.12	0.13	0.12	0.15	0.10	0.09	0.13
MgO	11.5	11.5	11.2	10.4	11.1	9.49	11.7	11.4	11.1	11.2	10.5	11.7	10.9
CaO	11.4	11.0	11.0	11.6	11.3	12.0	11.1	11.3	11.3	11.3	12.0	11.9	11.8
Na_2O	0.49	0.49	0.48	0.55	0.57	0.60	0.52	0.48	0.54	0.58	0.76	0.64	0.62
K_2O	0.32	0.34	0.29	0.35	0.39	0.43	0.31	0.31	0.36	0.43	0.29	0.30	0.31
Cr_2O_3	0.25	0.26	0.30	0.27	0.27	0.24	0.27	0.27	0.28	0.27	0.15	0.16	0.19
P_2O_5	0.16	0.22	0.14	0.19	0.12	0.17	0.20	0.22	0.20	0.16	0.41	0.25	0.31
Total	100.63	99.90	99.37	100.95	100.39	100.19	99.81	100.55	100.31	100.57	100.07	100.10	100.13
Number of spots analysed	2	20	7	9	10	5	24	67	31	18	14	4	7

[1]C—cryptocrystalline; NV—nonvesicular; SV—slightly vesicular; V—vesicular; (VAR)—variolitic; (F)—relatively fine grained; (M)—relatively medium grained; (C)—relatively coarse grained; BFC—within 60 μm of edge of felsite clast. Sample numbers are thin section numbers; parent piece for thin section is given in parentheses.

[2]From James (1976). Analyses were done at University of New Mexico by G. H. Conrad and K. Keil; SiO_2 and MgO values tabulated here have been corrected for systematic interlaboratory biases.

Table 5: Major and trace element chemistry of clasts in 73255.

Split	27,76,1	27,25,1	27,109	8,1	27,101,7	253,12,1	228,13,5	27,12,2	27,48,7	154,1,2	27,65,2,1	27,65,2,2	,27,45
	Bas	Bas	+100,1	Anor	Anor	Gab-an	An-gab	An-gab	An-gab	An-gab	Nor	Nor	Nor
wt%			Bas										
SiO_2	(43.6)	(46.1)	(52.9)	(43.0)	(45.5)	(45.9)	(46.9)	(47.1)	(46.1)	(46.6)	(51.1)	(49.8)	
TiO_2	2.1	1.54	0.34	0.02	0.27	0.10	0.26	0.18	0.28	1.47	0.68	0.52	
Al_2O_3	14.2	13.8	14.2	31.3	27.4	29.7	25.0	25.5	28.1	19.9	9.5	15.0	
Cr_2O_3	0.51	0.46	0.72	0.056	0.10	0.07	0.181	09	0.102	0.297	0.30	0.23	
FeO	16.6	17.1	15.4	3.24	7.9	4.4	6.7	6.6	6.3	9.4	12.1	9.2	
MnO	0.26	0.26	0.23	0.05	0.05	0.06	0.08	.06	0.055	0.127	0.18	0.14	
MgO	11.0	9.5	10.1	3.24	7.9	4.4	6.7	6.6	6.3	9.9	18.7	14.8	
CaO	11.5	11.0	10.0	18.7	14.0	15.9	14.8	14.9	14.5	11.6	7.1	9.8	
Na_2O	0.23	0.26	0.18	0.37	0.36	0.39	0.33	0.37	0.42	0.47	0.34	0.46	
K_2O				0.04						0.28		0.08	
P_2O_5													
ppm													
Sc	52.9	63.4	51.5	5.44	5.7	7.7	11.7	8.0	7.9	22	21.9	15.9	
V	120	160	220				35	24	18	78	78	58	
Co	26.5	22	36	6.48	24	4.2	20	32	18	26	23	20	
Ni				24	320	50	190	440	115	130	35	35	
							154	511					
Rb													
Sr		50	95		220	180	130			190	140	135	
Y													
Zr													
Nb													
Hf	1.55	1.51	0.45	0.58	1.2	0.98	0.96	1.1	3.5	7.5	1.8	0.9	
Ba					65		40	60	100	210	80	50	
Th		0.28		0.27	1.0	0.63	0.55	0.9	2.5	3.2	1.4	0.37	
U							0.025	0.027					
Cs													
Ta		0.30			0.36		0.18	0.2	0.6	1.1	0.14	0.14	
Pb													
La	1.82	2.75	0.92	1.67	2.92	1.79	2.32	3.0	7.9	16.7	9.77	3.15	
Ce	3.5	8.2	3.0	4.6	7.8	5.2	6.9	7.9	21.8	46	27	8.7	
Pr													
Nd	3.2	4.8			4.4	3.6	3.7	4.7	14	28	18	4.4	4.27
Sm	1.28	2.03	0.62	0.88	1.26	1.15	1.11	1.33	3.8	8.2	4.24	1.48	1.68
Eu	0.49	0.62	0.29	0.83	0.86	0.83	0.77	0.82	1.03	1.2	0.75	1.09	
Gd													
Tb	0.27	0.47	0.20	0.23	0.34	0.30	0.30	0.35	0.91	1.6	0.84	0.37	
Dy													
Ho													
Er													
Tm													
Yb	1.58	2.23	0.95	0.83	1.47	1.13	1.21	1.45	2.85	6.5	2.61	1.49	
Lu	0.30	0.36	0.16	0.12	0.22	0.17	0.18	0.22	0.42	1.0	0.38	0.22	
Li													
Be													
B													
C													
N													
S													
F													
Cl													
Br													
Cs													
Zn							1.71	1.92					
ppb													
Au							2.7	9.3					
Ir							6.5	21					
I													
At													
Ga													
Ge							75	172					
As													
Se							33	62					
Mo													
Te													
Ru													
Rh													
Pd							7.9	23					
Ag							0.56	0.77					
Cd							4.4	3.8					
In							<3	<2					
Sn													
Sb							2.5	1.68					
Te													
W													
Re							0.582	2.0					
Os							8.3	26					
Pt													
Hg													
Tl							0.89	1.35					
Bi							0.37	0.30					
	(1)	(1)	(1)	(1)	(1)	(1)	(1)	(1)	(1)	(1)	(1)	(1)	(2)

References and methods:
(1) Blanchard and Budahn (1979a,b); INAA (SiO_2 by difference)
except (a) Morgan and Petrie (1979a,b); RNAA
(2) Carlson and Lugmair (1981); ID/MS

Notes: The norites are all the same clast.

Table 6: Description of samples listed in Table 5.

Type sample number	Analyzed sample number	Sample descriptions
		Basalts
27,76	27,76,1	Single, clean piece of vuggy basalt (6.69 mg)
27,24	27,25,1	Basalt chip, black vuggy (9.33 mg)
27,105	(27,109) (110,1)	Coarser grained basalt, subophitic, vuggy (3.87 mg)
		Anorthosites
	8,1	Anorthosite analyzed in 1974; major elements by AAS
27,101	27,101,7	White material from the black and white nodule (see 27,101,10 for black) (9.96 mg)
		Gabbroic Anorthosite
253,12	253,12,1	3 plagioclase clasts (13.5 mg) from coherent gabbroic anorthosite clast
		Anorthositic Gabbros
228	228,13,5	Fine-grained, sugary clean piece of G–A (22.72 mg)
27,1	27,12,2	Fine-grained, sugary clean piece of G–A (30.70 mg)
27,48	27,48,7	Medium-grained, clean G–A (23.66 mg)
154,1	154,1,2	Very fine-grained G–A (8.32 mg)
		Norite
27,45	27,65,2,1	Clean sample of granulated, coarse-grained norite (12.91 mg)
27,45	27,65,2,2	Norite chip same as 27,65,21 but containing black veins (10.63 mg)
		Felsite
27,3	27,3	2 mg sample of hand picked, clean felsite and felsite and felsite glass
		Plagioclase
27,95	27,95,1	Pure plagioclase sample (3.9 mg)
27,80	27,80,1	Hand picked plagioclase separate from coarse grained pyroxene anorthosite—very clean (2.5 mg)
		Pyroxene
27,80	27,80,2	Hand picked pyroxene separate from coarse grained pyroxene anorthosite—probably not pure (0.7 mg)

The other highland breccia samples analyzed appear to be fairly typical lunar anorthositic breccias and feldspathic impactites, contaminated with meteoritic siderophiles. They have low rage earth abundances and positive Eu anomalies (Fig. 13a). One (, 154, not shown on Fig. 13a) is like a "very high alumina basalt" and appears to be an impact melt. Two of the feldspathic impactites ("anorthositic gabbros") were analyzed for meteoritic siderophiles and volatiles and appear to be, different in total abundance but fall in the same group 3 inferred to be a pre-Serenitatis meteoritic component (Morgan and Petrie, 1979 a, b).

RADIOGENIC ISOTOPES AND GEOCHRONOLOGY

^{4O}Ar-^{39}Ar stepwise beating analyses on several samples of aphanitic melt breccias were conducted by Jessberger et al. (1978) and Staudacher et al. (1979a, b); a single sample was similarly analyzed by Eichorn et al. (1979a, b), who also included aphanitic melt phases in their laser pulsed Ar study of materials in 73255. Jessberger et al. (1978) analyzed four samples of different aphanite types, summarized in Table 7 and Fig. 15. The apparent age spectra all show some structure, with clear low-temperature argon loss, then a low temperature "plateau" succeeded by a dip then a high-temperature "plateau". The low temperature "plateau" indicates a slightly younger age than the high temperature one (Table 7). The preferred interpretation of the authors is that the high-temperature region dates clasts and the low temperature region the melt; the dip might be a recoil effect. There are no clear differences between the melt age for vesicular and non-vesicular samples, but the vesicular samples appear to contain clasts that are much more degassed than those in the non-vesicular melts. Jessberger et al. (1978) conclude that the age of the melt and breccia forming event is 3.88 +/-0.03 Ga. Staudacher et al. (1979a, b) analyzed four more aphanitic melts (Tables 8 and 9 and Fig. 16), with similar results, and further discussed the significance of the structure in the temperature releases. The age inferred for the melt, i.e. the low-temperature

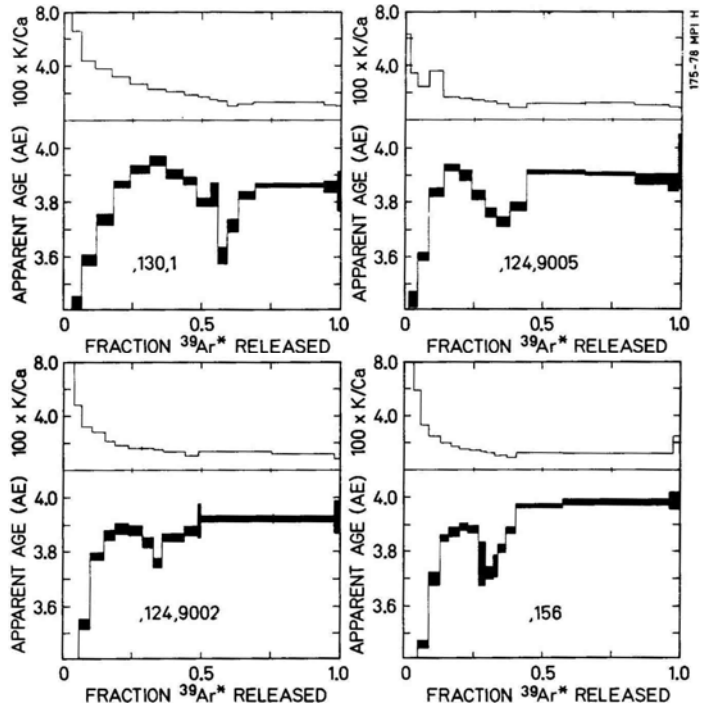

Figure 15: Ar-Ar and K/Ca release diagrams for 73255 aphanitic melts. Vesicularity decreases from top left to bottom right. Jessberger et al. (1978).

"plateau', depends on the model used to understand the structure, as listed in Table 9. In model A the dip is explained by gas loss from in model B the dip results from recoil from the fine-grained groundmass and results in slightly younger ages for breccia formation. Eichorn et al. (1979a, b) analyzed one sample of aphanite and obtained a roughly similar release structure (Fig. 17), although the dip is not so prominent. The precise age of the melt is difficult to infer from this release.

Eichorn et al. 1979a, b) used laser release from polished surfaces to obtain gas for Ar analyses of various phases in 73255. Samples were pre-heated to remove low-temperature gas, and the data correspond with K-Ar ages of an assumed higher-temperature plateau (assuming therefore no structure in the high-temperature release) because temperature cannot be controlled in this experiment. The inferred age data for the aphanites (included in the summary Table 10) are varied and determination of the age of the breccia-forming event is difficult at best. Clearly much material did not

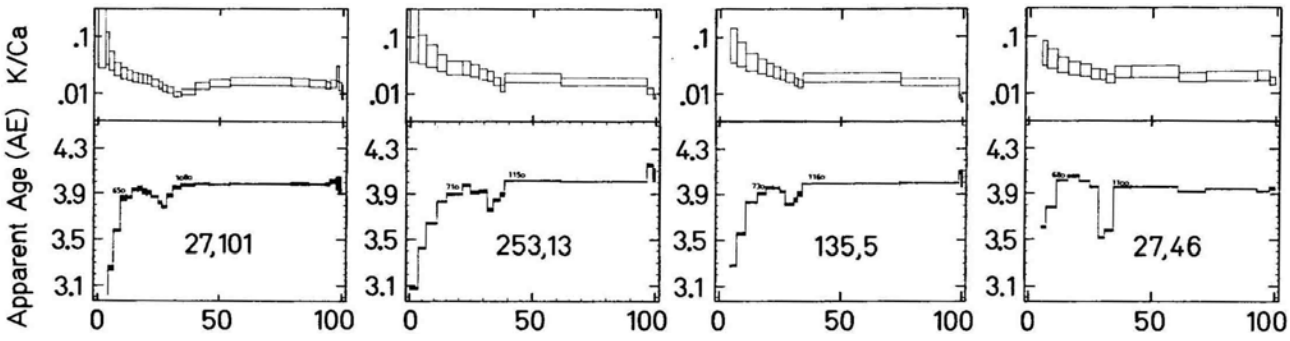

Figure 16. Ar-Ar and K/Ca release diagrams for 73255 aphanitic melts. Staudacher et al. (1979a).

Table 7: Summary of Ar-Ar release age data for 73255 aphanitic melts. , 156 is non-vesicular core; ,124,9002 Is a less-vesicular core/rind boundary sample; ,124,9005 is a more-vesicular core/rind boundary; ,130,1 is vesicular rind. Jessberger et al. (1978).

Sample Subnumber	K [ppm]	Ca [%]	Exposure Age[a] [m.y.]	K-Ar Age[b] [AE]	[AE]	^{40}Ar-^{39}Ar Plateau Ages[c]	Temperature Ranges
					Plateau 1	Plateau 2	^{40}Ar-loss corrected K-Ar Age
,156	1090	8.0	104	3.90	3.88 ± .02(670–810)	3.98 ± .01(1160–1440)	3.94 ± .03(670–1440)
,124,9002	1420	9.6	99	3.89	3.88 ± .02(700–820)	3.92 ± .01(1150–1400)	3.90 ± .02(700–1400)
,124,9005	1280	9.9	93	3.84	3.92 ± .02(720–780)	3.91 ± .01(1140–1410)	3.89 ± .03(720–1410)
,130,1	1350	7.7	86	3.80	3.90 ± .03(670–860)	3.86 ± .01(1160–1360)	3.86 ± .03(670–1360)

[a] Error is 15 m.y.
[b] Absolute uncertainty is 0.03 AE (1σ).
[c] Uncertainties listed are 2 σ and appropriate for comparison of the results within this study. Plateau ranges are given in brackets.

Table 8: Summary of Ar-Ar release age data for 73255 aphanitic melts and clasts. Plateau 2 is the high-temperature region inferred to represent clasts. Staudacher et al (1979a).

Sample subnumber		K [ppm]	Ca [%]	Exposure Age[a] [m.y.]	K-Ar age[b] [AE]	^{40}Ar-^{39}Ar age[d] Plateau 1[c] [AE]	Plateau 2 [AE]
253,13	aphanite coating	1380	7.2	97	3.92		4.00 ± .01
135,5	aphanite in mottled lithology	1430	7.2	96	3.89		3.99 ± .01
27,101	aphanite from black and white nodule	1130	7.3	92	3.89		3.99 ± .01
27,46	aphanite coating	1670	7.4	94	3.87		3.94 ± .01
156[+]	nonvesicular core aphanite	1090	8.0	96	3.90		3.98 ± .01
124,9002[+]	less vesicular aphanite from core-rind contact	1420	9.6	91	3.89		3.92 ± .01
124,9005[+]	more vesicular aphanite from core-rind contact	1280	9.9	86	3.84		3.91 ± .01
130,1[+]	highly vesicular rind aphanite	1350	7.7	79	3.80		3.86 ± .01
228	anorthositic gabbro clasts	450	9.7	92	3.95	3.96 ± .01	4.20 ± .01
27,1,2		600	9.2	94	3.90	3.93 ± .01	4.14 ± .02
27,1,1		630	10.1	88	3.85	3.91 ± .02	—
27,48		590	9.7	89	3.89	3.93 ± .02	—

[a] Error is 10 m.y.
[b] Absolute uncertainty is .03 AE
[c] Low temperature ages for aphanites are listed in Table 3.
[d] An absolute error of ±.03 AE is not included.
[+] Results are taken from Jessberger *et al*. (1978).

Table 9: Model ages for low temperature regions of Ar-Ar release data for 73255 aphanitic melts. Temperature range for corresponding fractions given in parentheses. Staudacher et al. (19798).

Sample subnumber	Model A Age Plateau 1 [AE]	Model B Age [AE]	^{39}Ar redistribution in Region I [%]
73255,253,13	3.92 ± .02 (710–900)	3.89 ± .03 (710–1080)	1.2
135,5	3.93 ± .02 (730–880)	3.90 ± .02 (730–1090)	1.4
27,101	3.90 ± .02 (650–890)	3.88 ± .02 (650–1010)	1.1
27,46	4.01 ± .02 (680–890)	3.89 ± .09 (680–1030)	5.1
156	3.88 ± .02 (670–810)	3.83 ± .03 (670–1010)	1.7
124,9002	3.88 ± .02 (700–820)	3.85 ± .02 (700–1030)	.8
124,9005	3.92 ± .02 (720–780)	3.82 ± .04 (720–1060)	2.0
130,1	3.90 ± .03 (670–860)	3.85 ± .04 (670–1080)	2.2

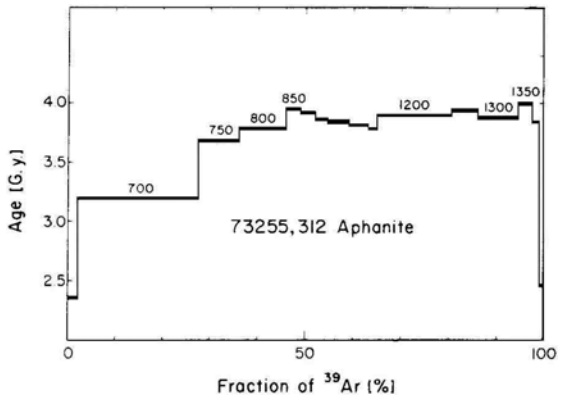

Figure 17: Ar-Ar release diagram for a 73255 aphanitic melt. Eichorn et at (1979a).

Completely degas at the time of melting, which is best inferred from the best-degassed clasts and the thermal releases (such as those of Staudacher et al. (1979a) which agree at 3.87 +/- 0.03 Ga.

James et al. (1978) reported Rb and Sr isotopic data on 7 aphanitic melt phases from 73255. Calculated to about 3.9 Ga, the data show that there were significant differences in $^{87}Sr/^{86}Sr$ at that time (Fig. 18), thus the melt did not then equilibrate over a scale of a few millimeters. The data indicate similarities with other aphanitic melts (Fig. 18) with the bulk data reflecting mixing of materials.

Staudacher et al. (1979a, b) conducted thermal release Ar-Ar studies on clasts in 73255: one felsite and three "anorthositic gabbros" (one duplicate). The data ate summarized in Table 8 and the release diagrams shown as Fig. 19 (anorthositic gabbros) and Fig. 20 (felsite). Two of them (,228 and one chip of 27,1 are stated to have a marked 2-step release, with low temperature release indicating lower ages. The other two show low temperature releases that rise more gradually to high-temperature, higher ages (Fig. 19). The felsite (Fig. 20) is the same clast analyzed by Blanchard and Budahn (1979a, b); it shows a high-temperature plateau age of 3.89 +1-0.03 Ga over the last 50% of Ar release. This is inferred to date the melting and degassing of the felsite as it was incorporated into the melt, thus dating the melt event.

Eichorn et al. (1979a, b) used laser release from polished surfaces to obtain gas for Ar analyses of various phases in 73255. Samples were pre-heated to remove low-temperature gas and the data correspond with K-Ar ages of an assumed higher-temperature plateau (assuming, therefore, no structure in the high-temperature release) because temperature cannot be controlled in this experiment. The inferred age data for the clasts are summarized in Table 10. They show a wide variety of ages, including some that are rather younger than the inferred age of the host melt, e.g. felsites range from 3.48 to 3.98 Ga. Devitrified maskelynites give "ages" as old as 5.5 Ga (Table 12), hence maskelynites must be considered unreliable for determining ages. No other samples except some groundmasses suggest ages older than 4.0 Ga.

Carlson and Lugmair (1981) reported a Sm-Nd isotopic analysis of the pristine igneous gabbronorite ,27,45 (Table 13, Fig. 21). The three-point isochron gives an age of 4.23 +/-0.05 Ga and is well defined. The T_{ICE} age is similar to the isochron age, thus the

Table 10: Summary of laser Ar ages (Ga) in 73255, for melt and clasts (preheated samples).
Eichorn et al. (1979a).

Sample	Preheating temperatures[1] 650°C	700°C	900°C
	Groundmass		
73255,255			
nonvesicular	4.10 ± .01	4.09 ± .03*	4.21 ± .01*
(~ 2 μm grain size)	4.07 ± .01*		4.03 ± .01*
	4.00 ± .01		
cryptocrystalline			4.02 ± .01*
(< 1 μm grain size)			
73255,310			
highly vesicular	3.76 ± .01	3.78 ± .01*	3.86 ± .03*
(~ 4–5 μm grain size)	3.80 ± .01*		
	3.78 ± .01		
slightly vesicular			3.91 ± .02*
(~ 2 μm grain size)			
73255,309			
fine-grained (~ 1 μm)	3.91 ± .01	4.09 ± .01	4.07 ± .01
coarse-grained (5–10 μm)	3.80 ± .01	3.81 ± .01	3.70 ± .02
	Felsic clast material		
73255,255			
glass A	3.77 ± .01	3.72* ± .01	3.73* ± .01
	3.58* ± .01		
K-feldspar A	3.96 ± .01	3.93* ± .01	3.92* ± .01
	3.98* ± .01		
K-feldspar C	3.94 ± .02		
K-feldspar B			3.73 ± .03
73255,310			
partly melted			
vermicular intergrowth C	3.72 ± .01		3.97 ± .02*
	3.69* ± .01		
partly melted			
vermicular intergrowth I	3.77 ± .01	3.82 ± .02*	
glass H	3.69 ± .01		3.87 ± .02*
plagioclase H	3.87 ± .03		
partly melted			
vermicular intergrowth D			3.86 ± .02*
vermicular intergrowth F			3.48 ± .03*
73255,312			
glass D	3.59† ± .01		
	Lithic clasts		
ANT-suite fine-grained anorthositic gabbro			
73255,310			
shocked clast M	3.81 ± .01		
small plagioclases in clast J	3.74 ± .01	3.84* ± .02	
large plagioclases in clast J	3.93 ± .01		

Table 10: Continued.

Sample	Preheating temperatures[1] 650°C	700°C	900°C
Lithic clasts			
73255,309			
clast B	3.67 ± .01	3.77 ± .05	
73255,312			
clast B	3.73† ± .01		
ANT-suite coarse-grained pyroxene anorthosite			
73255,309			
relict plagioclase of clast D	3.66 ± .02		} 3.92 ± .08
shattered plagioclase of clast D	3.62 ± .02		
Fine-grained quenched basalt			
73255,309			
Groundmass A1	3.84 ± .01	3.81 ± .01	
Groundmass A2			3.99 ± .01
Devitrified maskelynite clasts			
73255,255			
Centers of two 0.5-mm clasts	3.99 ± .01		
73255,310			
center of 0.3-mm clast A	3.99 ± .01		
center of 0.5-mm clast B	4.82 ± .02		
	4.96* ± .05		
intermediate zone within 0.5-mm clast B	4.34 ± .03		
	4.36* ± .04		
centers of 5 0.2-mm clasts	3.89 ± .01		
73255,309			
center of 0.3-mm clast	4.14 ± .02	4.20 ± .02	

[1] Samples were preheated for 1.5 hours at each temperature successively. Ages marked with an * were obtained on samples that were preheated twice, for a total of 3 hours, at 650°C. Ages

Table 11: Rb-Sr isotopic data for 73255 aphanites. James et. al (1978).

Sample	Rb (ppm)	Total Sr (ppm)	$^{87}Rb/^{86}Sr$	$^{87}Sr/^{86}Sr$
Vesicular rind aphanite				
122	9.85	128.6	0.2214	0.71251
Slightly vesicular aphanite, at core-rind contact				
9006 (110)	9.93	126.1	0.2276	0.71287
9004 (124)	5.47	126.0	0.1254	0.70705
Nonvesicular aphanite				
9003 (124)	5.56	127.3	0.1261	0.70698
9007 (148)	5.31	122.8	0.1248	0.70679
176	5.54	125.4	0.1276	0.70701
9008 (245)	5.28	118.1	0.1291	0.70723

Table 12: Summary of laser-released Ar studies of a 1.4 mm clast of denitrified maskelynite in 73255. Eichorn et al. (1979a).

	Center	Zone 4	Zone 3	Zone 2	Edge
Surface 1	4.20 ± .05	4.03 ± .01	4.49 ± .02	4.51 ± .02 4.20 ± .01	4.13 ± .01
Surface 2	3.99 ± .02	4.39 ± .02	4.26 ± .01	4.96 ± .02	4.02 ± .02
Surface 3	3.99 ± .01	4.01 ± .01	3.99 ± .02	5.53 ± .01	5.68 ± .02

Table 13: Sm-Nd isotopic data for mineral separates and whole rock of 27.45 gabbronorite. (Carlson and Lugmair, 1981)

	Center	Zone 4	Zone 3	Zone 2	Edge
Surface 1	4.20 ± .05	4.03 ± .01	4.49 ± .02	4.51 ± .02 4.20 ± .01	4.13 ± .01
Surface 2	3.99 ± .02	4.39 ± .02	4.26 ± .01	4.96 ± .02	4.02 ± .02
Surface 3	3.99 ± .01	4.01 ± .01	3.99 ± .02	5.53 ± .01	5.68 ± .02

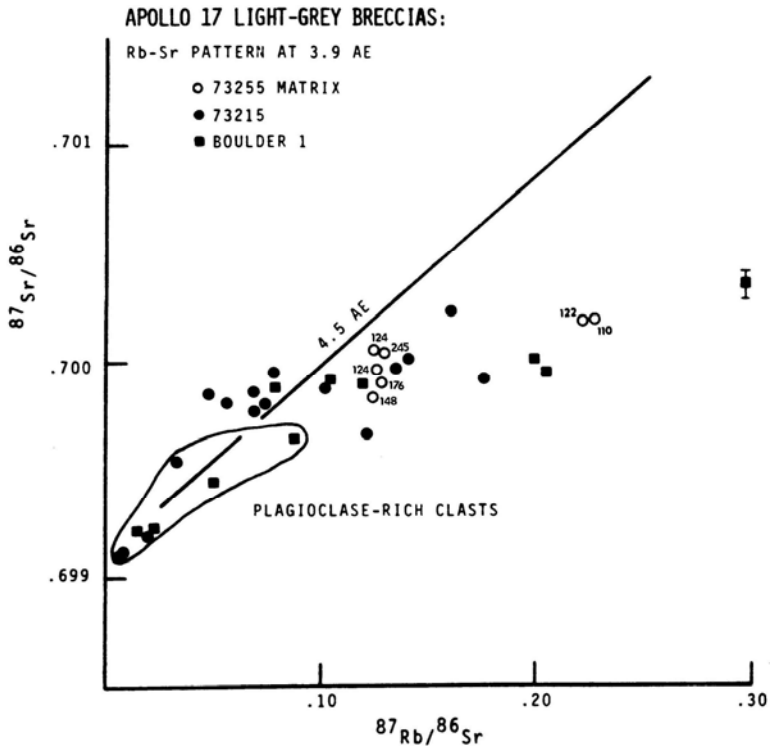

Figure 18: Modified Sr evolution diagram for samples from. Apollo 17aphaniticmelt rocks. The diagram shows how the pattern would have appeared if measured just after the breccias formed about 3.90 Ga ago. James et al. (1978).

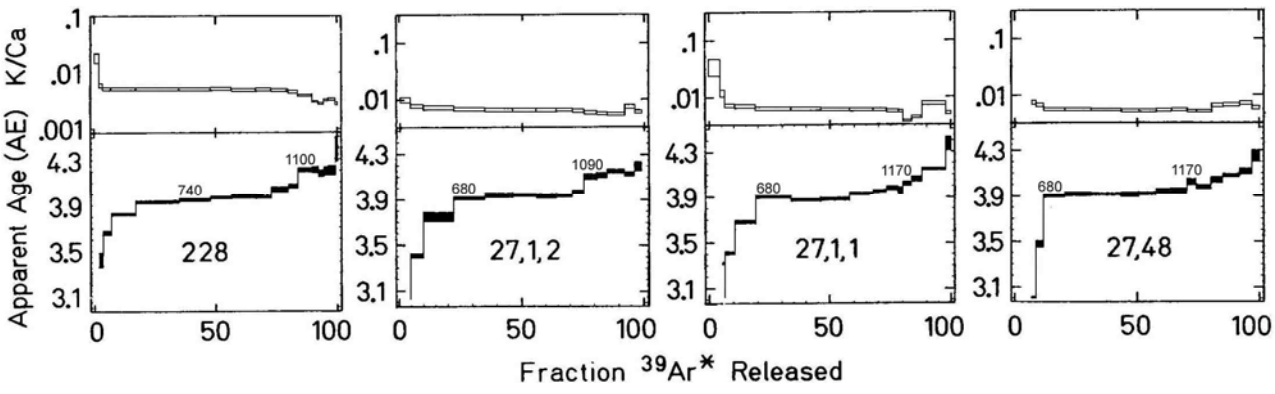

Figure 19: Ar -Ar and K/Ca release diagrams for "anorthositic gabbro" clasts in 73255, including 2 splits of a single sample. Staudacher et al. (1979a).

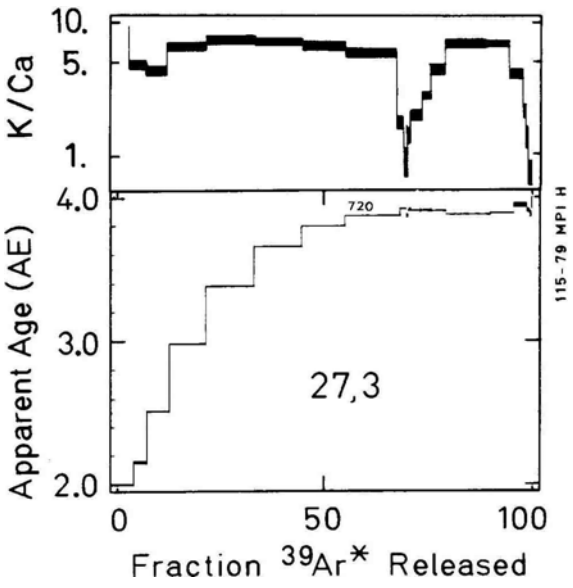

Figure 20. Ar-Ar and K/Ca release diagram for a felsite clast in 73255. Staudacher et al. (1979a).

granulation and breccia formation did not disturb the Sm-Nd system. Sources at 4.23 Ga had not sufficiently fractionated Sm/Nd or had not existed long enough to evolve a Nd isotopic signature reasonably different from the assumed chondritic reference. This implies that liquids with highly fractionated relative rare earths were crystallizing to produce melts of the Mg-suite 4.2 to 4.3 Ga ago.

EXPOSURE AGES

Microcraters on the surface of 73255 are sparse and tiny on all surfaces, and nowhere approach saturation. The uniform coverage shows that the sample must have been tumbled at least once (James and Marti, 1977).

Exposure ages have been determined from the Ar isotopic studies. Staudacher et al. (1979a, b) listed exposure ages for clasts and aphanitic melts (Table 8) that include revisions (apparently corrected for Ti- and Fe-contributions to the ^{38}Arc production) of the exposure ages reported for four aphanitic melts by Jessberger et al. (1978). These exposure ages average 91 Ma with a range from 71 Ma to 97 Ma. The laser study of Eichorn et al. (1979a) produced a similar range of Ar exposure ages for clasts and aphanitic melts (86-104 Ma, average about 97 Ma). The stepwise heating experiment on a single sample of aphanitic melt produced a similar exposure age. This age has occurred for other landslide samples and is inferred to be the age of the landslide.

James and Marti (1977) reported an ^{81}Kr-^{83}Kr age of 149 Ma for an interior, non-vesicular aphanitic melt. This age is substantially older than the Ar exposure ages. The high spallation ^{78}Kr/^{S3}Kr suggests little shielding during exposure and the xenon isotopes too suggest that the entire radiation took place within a few centimeters of the surface.

Yokoyama et al. (1974) found that 73255 was saturated with both ^{22}Na and ^{26}A1, thus the sample has been exposed for at least a few million years.

PROCESSING

Following separation of a few small pieces for preliminary study, a slab about 1.5 cm thick was sawn through 73255 (Figs. 2,4) in 1974 for the consortium study led by O. James. Butt end piece ,17 (Fig. 3) remains intact at 102 g. Some further processing of butt end piece ,12 (Fig. 2) was done but its mass too remains close to the original at 127 g. The slab piece, consisting mainly of ,27; ,20; and,29 has been extensively subdivided and many allocations made from both interior and exterior parts. More than 100 thin sections or probe mounts have been made from many different pieces of 73255.

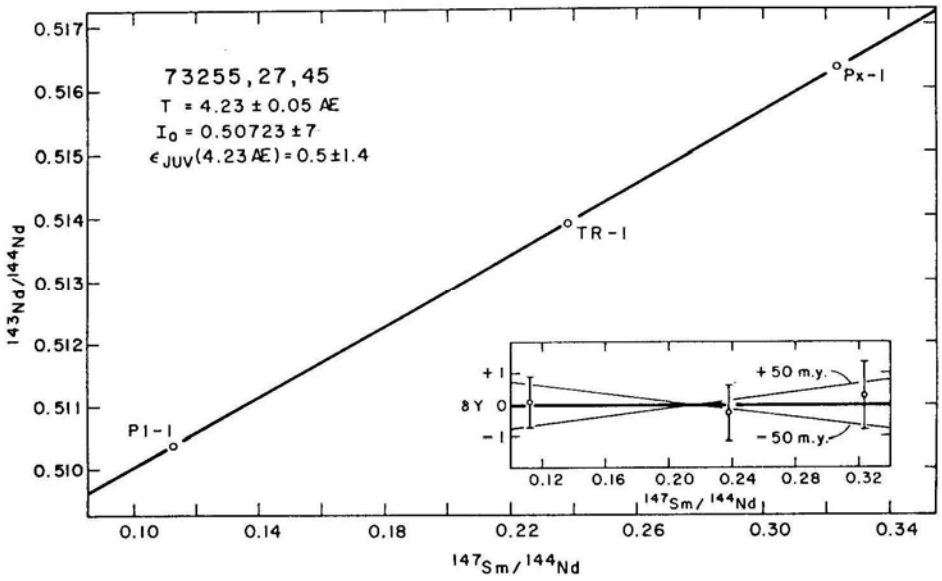

Figure 21: Sm-Nd isochron for gabbronorite, 27, 45. Carlson and Lugmair (1981).